



PCCP

Impact of Pore Size, Interconnections, and Dynamic Conductivity on the Electrochemistry of Vanadium Pentoxide in Well Defined Porous Structures

Journal:	<i>Physical Chemistry Chemical Physics</i>
Manuscript ID	CP-ART-07-2018-004706.R1
Article Type:	Paper
Date Submitted by the Author:	11-Oct-2018
Complete List of Authors:	Kim, Nam; University of Maryland, Department of Chemistry and Biochemistry Sahadeo, Emily; University of Maryland at College Park, Chemistry and Biochemistry Liu, Chanyuan; Lam Research Corp Rose, Olivia; University of Maryland, Department of Chemistry and Biochemistry Rubloff, Gary; University of Maryland, Department of Materials Science and Engineering; University of Maryland, Institute for Systems Research Lee, Sang Bok; University of Maryland, Department of Chemistry and Biochemistry; University of Maryland, Department of Materials Science and Engineering; Korea Advanced Institute of Science and Technology, Graduate School of Nanoscience and Technology

SCHOLARONE™
Manuscripts



Journal Name

ARTICLE

Impact of Pore Size, Interconnections, and Dynamic Conductivity on the Electrochemistry of Vanadium Pentoxide in Well Defined Porous Structures

Received 00th January 20xx,
Accepted 00th January 20xx

DOI: 10.1039/x0xx00000x

www.rsc.org/

Nam Kim^a, Emily Sahadeo^a, Chanyuan Liu^b, Olivia Rose^a, Gary Rubloff^{c,d}, Sang Bok Lee^{*a,c,e}

Considering the tortuous, random porous nanostructures existing in many battery electrodes, it is essential to understand electronic and ionic behaviors in such a confined nanoscale porous geometry in which electron and ion transports can change dynamically. Here, we have carefully designed three dimensional (3D) interconnected porous electrode structures and performed experiments to probe how the ion and electron transport is impacted within these controlled geometries. By using anodized aluminum oxide as a template, we were able to fabricate both 1D array electrodes and 3D electrodes with varying numbers of interconnections, utilizing vanadium oxide (V_2O_5) as the active material. We demonstrate that the inherent properties of the electrode material in combination with the structural properties of the electrodes can both positively and negatively impact electrochemical characteristics. Most notably, electrodes with seven interconnecting layers in their structure had 19.7% less capacity at 25C than electrodes with zero interconnecting layers, demonstrating the negative effect of interconnections combined with poor electronic conductivity of V_2O_5 upon lithiation beyond one Li insertion. These results indicate that a careful consideration of the material and structural properties is needed for the design of high performance battery systems.

1 Introduction

With the increased demand for high performing energy storage devices, researchers all over the world are focusing on improving the energy densities, power densities, and cycle life of various energy storage devices.¹⁻⁷ Due to their superior energy storage performance, lithium ion batteries are often chosen for portable devices.⁸⁻¹¹ Commercialized lithium ion batteries are traditionally made of composite electrodes using electroactive particle sizes ranging from microns to nanometers mixed with conductive additives and binders. Due to the non-uniformity of the particles and non-uniform mixing of the conductive additives and binders, differences in the local tortuosity, porosity, and conductance within the electrodes are inevitable, which causes differences in ionic and electronic transport.¹²⁻¹⁵ The electronic conductivity of the electroactive materials are often not static during the lithiation and delithiation steps of battery cycling. For example, lithium cobalt oxide, when fully lithiated, has electronically insulating

properties. However, as it is delithiated the material becomes more electronically conducting.¹⁶ In another material, manganese dioxide, as it is lithiated it becomes more electronically conducting.¹⁷

The randomness of the electrode morphology combined with the dynamic properties of the electrode material makes understanding their impact on the electrochemistry difficult. Initial studies on understanding the origin of battery performance (power density, energy density, and cycle life) was based on the use of homogenous spherical particles such as the Newman model. While this model can predict the energy and power density of the electrode, due to its low-dimensional nature this model would need to be much more complicated to explain the degradation mechanisms in real battery electrodes; the electrode structures used in the model are overly simplified. Using focused ion beam, or X-ray tomography, several studies were carried out using the real electrode structures as the basis for the modelling of the battery performance with a small section (few thousands of cubic μm) of the total battery electrode.^{12-15, 18} Another approach in understanding how the local electrode structure impacts the electrochemistry is to fabricate well controlled uniform testbed electrodes with controlled structural properties such as tortuosity and porosity.

In order to fabricate well controlled electrode structures, we used anodized aluminum oxide (AAO) as a template. With the right combination of the temperature, anodization voltage, and electrolyte, a uniform, porous aluminum oxide layer can be formed.^{19, 20} In traditional AAO structure, cylindrical pores are formed in a hexagonal pattern perpendicular to the surface.

^a Department of Chemistry, University of Maryland, College Park, MD, 20740, USA.
Email: slee@umd.edu

^b Lam Research Corp, Tualatin, OR 97062, USA

^c Department of Material Science and Engineering, University of Maryland, College Park, MD 20740, USA.

^d Institute for Systems Research, University of Maryland, College Park, MD, 20740, USA

^e Graduate School of Nanoscience and Technology, KAIST, Daejeon 305-701, Korea

^f † Electronic Supplementary Information (ESI) available: [Experimental methods, Pore size variation of the AAO templates before and after ALD, image of AAO at various stages of preparation]. See DOI: 10.1039/x0xx00000x

Atomic layer deposition can be used to conformally deposit electrode materials in these high aspect ratio structures.²¹ This methodology results in nanotubular array electrodes, with each electrode electronically and ionically isolated from one other. The AAO template structure can be varied by introducing interconnections between adjacent pores during the anodization process.²²⁻²⁴ The electrode structure resulting from this interconnected template has additional electronic and ionic pathways between adjacent electrodes. These interconnecting layers can be introduced into the AAO template controllably by simply varying the anodization voltage.

In our previous study, we focused on how different numbers of interconnecting layers, which introduced additional electronic and ionic pathways, as well as structural irregularities had an impact on the electrochemistry of the vanadium pentoxide (V_2O_5).²⁵ In this study, the number of interconnecting layers was varied from zero (straight) to three interconnecting layers within about 1.7 μm thick AAO films. These AAO films were used as a scaffold for nanotubular V_2O_5 electrodes. Each electrode was cycled within the one lithium insertion/deinsertion window (2.6V to 3.8V). An interesting phenomenon was observed where with more interconnecting layers, not only was the mass loading of the electrodes increased due to the increased surface area from the interconnections, but they also had increased capacity retention at high current densities. To understand how the interconnections impacted performance, the three types of transports (bulk ion transport, solid state ion transport, and electron transport) that govern the electrochemical reactions had to be deconvoluted experimentally. It was found that these interconnections allowed more active material closer to the planar current collector, leading to better material utilization at high current densities where the electron transport was the limiting mechanism.

In the aforementioned study, a more significant degradation of the interconnected electrodes over the straight electrodes was expected due to the increased structural irregularities of the electrodes at the interconnected regions.²⁶⁻²⁸ However, no significant degradation was seen between the two structures. This result suggests that the interconnecting layers likely did not cause inhomogeneous current distribution.²⁵ However, an alternate explanation may be that the ability of V_2O_5 to accommodate up to two lithium ions reversibly enabled the electrodes to be cycled without severe capacity degradation.²⁹⁻³¹ Within the one Li ion insertion window, the high current densities around the localized interconnected regions could result in a second Li ion insertion which is still reversible, resulting in no significant degradation compared to zero interconnecting layer electrodes. However, if a third lithium ion is inserted that process is irreversible³².

We initiated the study in this manuscript to explore whether high current density regions form due to structural irregularities at the interconnections, and if they subsequently drive further lithiation of V_2O_5 into a third electron transfer. In this work, we move beyond the one electron transfer window of lithium insertion and instead cycle V_2O_5 in the two-lithium insertion window. By going into the second Li insertion regime, at high

current densities it is possible that the structural irregularities from the interconnecting regions will cause a third Li ion to insert due to the overpotential needed to maintain the reaction current.³³ This third Li insertion is an irreversible reaction, which could degrade the electrodes with interconnecting regions faster than their straight pore counterparts or otherwise impact the electrode chemistry. Herein, we discuss how interconnections between AAO pores, the pore size, and changes in material conductivity influence the performance of V_2O_5 cathodes in the two-lithium insertion window.

Here we demonstrate that within our test structures, interconnecting regions have different impacts on the electrochemistry of the electrodes depending on the degree of lithiation. With only one Li insertion window, interconnected electrodes can maintain higher capacities at high current densities, as seen from the previous study. Conversely, within the two Li insertion window, interconnected electrodes maintain lower capacities at high current densities. We also demonstrate that the need for diffusion of the additional Li ions into the nanotubular pores does not cause this deviation in the two Li insertion window. By using an integrated current collector, we show that it is due to the synergy, both positive and negative, between the changes in the dynamic electronic conductivity of the V_2O_5 electrode and the interconnecting structure that impacts the overall conductance of the electrode. This finding suggests that in real commercial battery electrodes, when the active material does not have direct contact with the current collector, the active material usage at high current densities is maximized when there are additional electronic pathways in materials whose electronic conductivities increase with lithiation. However, material utilization is minimized when active materials have decreased electronic conductivities upon lithiation.

Results and Discussion

Template characterization

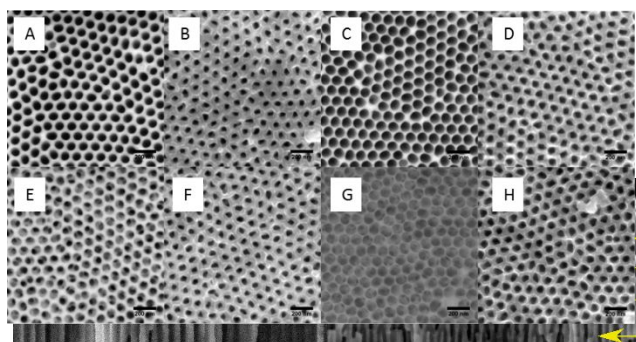


Fig. 2 SEM image of the top of AAO templates before and after deposition of 20nm thick V_2O_5 . Before (a) and after (b) deposition of zero interconnecting layers after 11.5 minutes of pore widening, before (c) and after (d) deposition of zero interconnecting layers after 15.5 minutes of pore widening, before (e) and after (f) deposition of seven interconnecting layers after 11.5 minutes of pore widening, and before (g) and after (h) deposition of seven interconnecting layers after 15.5 minutes of pore widening.

Fig. 1 Cross-sectional SEM images of AAO films with zero (left) and seven (right) interconnecting regions. The interconnecting regions are highlighted in yellow. Carbon was sputtered to minimize charging.

AAO templates with zero, four, and seven interconnecting layers were fabricated. Figure 1 shows representative SEM cross section images of AAO films with 0 and 7 interconnecting layers. The 7 interconnecting layers are evenly distributed in 2.3 μm thick AAO films, while the straight pores contain no interconnections but are of the same thickness. Due to the insulating nature of the AAO, carbon was sputtered to minimize charging on the surface during SEM imaging. To create the electrodes within the AAO template, a ~ 10 nm thick crystalline V_2O_5 film was deposited in the AAO templates using ALD. The successful deposition and its thickness was confirmed with SEM images of the AAO pore diameter before and after deposition as seen in Figure 2. Figure 2a,b and Figure 2e,f depict pores after 11.5 minutes of pore-widening, which gives pores 50 nm wide. This diameter is the pore size used for all tests in this study, except data where pores are denoted as being 61 nm in diameter. The 61 nm-wide pores are illustrated in Figure 2c,d and Figure 2g,h and underwent 15.5 minutes of pore widening prior to V_2O_5 deposition. Detailed size distribution of the pores before and after deposition can be found in the Supplementary Information. After deposition, gold was sputtered on top of the AAO as a planar current collector. Using Swagelok T-cells with two Li foils as separate reference and counter electrodes, V_2O_5 electrodes with varying numbers of interconnecting layers were tested.

Electrochemical Testing of Interconnected V_2O_5 Electrodes

To confirm the results from our previous study with the different number of interconnections chosen for this paper, V_2O_5 was cycled within the one lithium insertion window in electrodes with four and seven interconnections. From Figure 3a, it is apparent that with more interconnecting layers, better capacity retention was seen at higher current densities, which agrees with the previous findings.

After confirming the one-lithium insertion results, we then tested the impact of additional Li ion insertion into V_2O_5 electrodes with interconnecting layers. The electrochemical

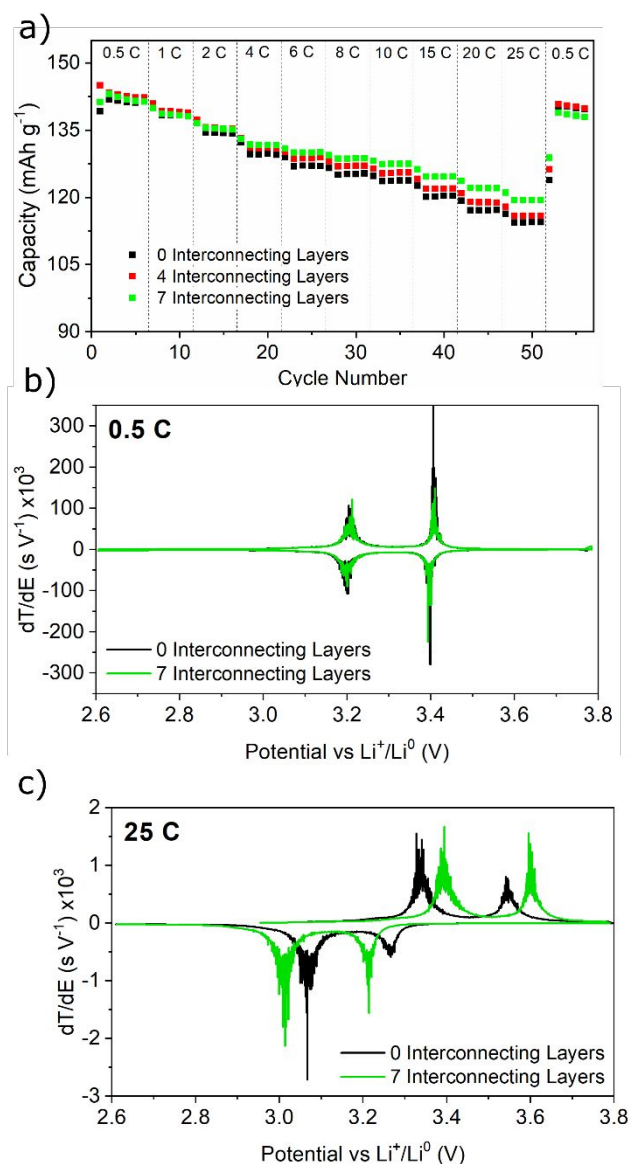


Fig. 3 (a) Capacity of V_2O_5 of electrodes with varying number of interconnecting layers, cycled between 2.6 V and 4 V vs Li. First derivative of the inverse voltage profile at (b) 0.5C and (c) 25C.

window was increased (3.8V to 2V vs Li), enabling a second electron transfer reaction to occur. As it can be seen in Figure 4a, at low current densities, the interconnections had no significant impact on the capacity of the electrode, as seen previously. However, when the current density was increased, the electrode with more interconnecting layers had lower capacity, which is the opposite of what was observed in the one-lithium insertion regime. The capacity, or the total material usage, at high current densities is limited either by the Li ion transport or electron transport, depending on the electrode structure and the active material. To deconvolute the ion and electron transport effects, we carefully designed experiments to probe these properties independently. The results of these tests are presented in the following sections.

Effect of Pore Size

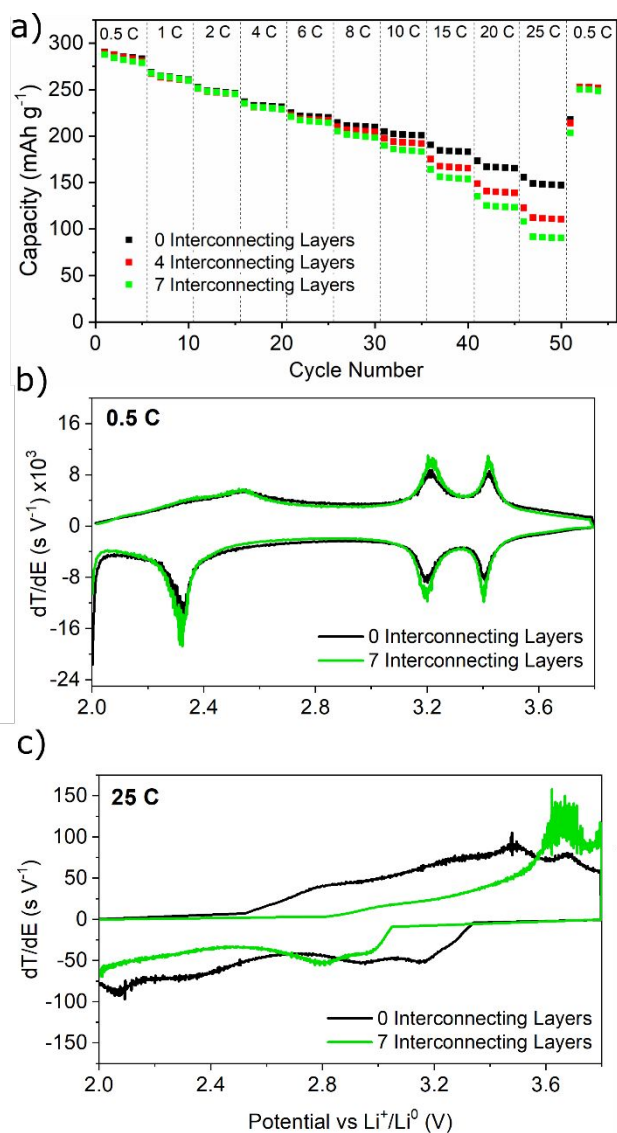


Fig. 4 (a) Capacity of V₂O₅ of electrodes with various interconnecting layers, cycled between 2 V and 4V vs Li. First derivative of the inverse voltage profile at b) 0.5C and c) 25C.

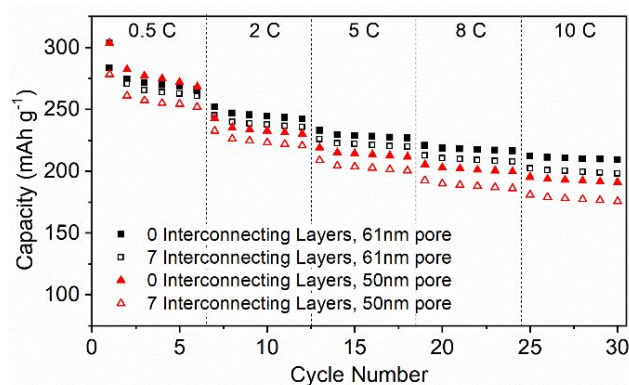


Fig. 5 Capacity of V₂O₅ of electrodes with various interconnecting layer with larger, 61nm pore, and smaller, 50nm, pore diameter openings at various current densities.

To determine if the performance of V₂O₅ electrodes in our set-up was limited by Li ion transport into the pores, we considered how the size of the pore opening may affect the results. Using the SEM images of the AAO top-view before and after deposition, pore diameters were analyzed using ImageJ software's Analyze Particle function. Additionally, the cross-section images of the AAO templates and the template thickness were used to determine the dimensions of the pores for the estimation of Li ion concentration in the pores. To estimate the amount of Li ions available in each of the pores and how many need to diffuse from the bulk of the electrolyte into the confined pore spaces for a two-Li insertion, a few assumptions were made for the calculations. The pores are assumed to be perfectly cylindrical and using the diameter of the AAO pore measured from the SEM images before and after ALD of V₂O₅, 70 nm and 50 nm respectively, the V₂O₅ thickness was found to be 10 nm. The length of the AAO was 2.3 μm and using these values the nanotubular electrode volume was estimated. Utilizing the bulk density of V₂O₅, 3.36 g cm⁻³ the total V₂O₅ in the pore was estimated.³⁴ The total number of Li ions in each of the pore was estimated by assuming that the internal volume of the tubular structure was still cylindrical. Utilizing the diameter of the pore opening after ALD, 50nm, and a depth of 2.3 μm from the cross-section images, the total volume of electrolyte was estimated. Assuming the initial concentration within the pore was the same as the bulk, 1M LiClO₄ in PC electrolyte, the total number of Li ions per pore was estimated. The amount of Li ions and V₂O₅ in each pore was estimated to be 8.01x10⁻¹⁷ moles of V₂O₅/pore and 4.52x10⁻¹⁸ moles of Li ion/pore at rest. To lithiate the V₂O₅ to Li₂V₂O₅, each V₂O₅ unit requires two Li ions, indicating 1.60x10⁻¹⁶ moles of Li ions are needed per pore. With only 4.52x10⁻¹⁸ moles of estimated Li ion/pore, which accounts for only 3% of the total required Li ions for two full lithiations of V₂O₅ in each of the pores, 97% of the required Li ions still need to diffuse from the bulk of the electrolyte into the confined pores of the V₂O₅ nanotube electrodes. At low current densities, the rate of depletion of Li ions within the pores and the diffusion of Li ions from the bulk into the pores may be similar, allowing full material usage. As the current density increases, the rate of Li ion depletion increases as well. However, the rate in which the Li ions can diffuse from the bulk into the pores is limited by the diffusion coefficient and the diffusional cross-sectional area, i.e.

the pore diameter, resulting in ion starvation where the ions are not diffusing fast enough to match the reaction rate. Kitada *et al.* and several other groups have shown that in highly confined electrode systems, it was the ion transport that was limiting the capacity at higher current densities.³⁵⁻³⁷ To explore the possibility of ion starvation in this system, the pore diameters were varied by changing the pore widening time of the AAO template. By altering the pore diameter, it is expected that a larger pore will be able to maintain larger ion transport capability than a smaller pore, due to the larger cross-sectional diffusional area.

With increased pore widening time, the final pore diameter was able to be increased from 50 ± 3 nm to 61 ± 4 nm. With the increased pore diameter, not only is the amount of Li ions available in the pore greater, but also the pore cross-sectional area is larger which increases the Li ion transport rate for Li ion diffusion from the bulk electrolyte into the pores. Figure 5 shows the resulting capacities of electrodes with larger 61 nm pores and smaller 50 nm pores. Current densities up to 10 C were chosen as it was enough to clearly show the difference in the impact of the pore diameters and interconnecting layers on the capacities. There was an increase in the capacity retention at various current densities with larger pore diameters, but the trend observed in Figure 4 where more interconnections showed higher capacity loss is maintained even in the electrodes with larger pore openings. Therefore, these results still do not explain the discrepancies between the one-Li and two-Li insertion electrochemical windows. This suggests that even 50 nm pore diameter is enough to support the ion transport needed for high current densities.

Effect of Dynamic V_2O_5 Conductivity

As V_2O_5 is a well-studied cathode material for Li-ion batteries, its electronic conductivity has previously been studied at various levels of lithiation.^{38, 39} The literature shows that the conductivity of V_2O_5 is dynamic with the degree of lithiation. While the absolute number of the conductivity varies from study to study, it is accepted that the conductivity reaches its maximum at about $Li_{0.5}V_2O_5$ and declines upon further lithiation yet remains in the same order of magnitude up to one full Li insertion, $Li_1V_2O_5$. With the second Li insertion, however, the conductivity drops by two orders of magnitude. Understanding that the conductivity of V_2O_5 is dynamic, both positive and negative synergistic behaviors between the interconnections and the degree of lithiation can be explained.

Pearse *et al.* used XPS to probe into the mechanism of inhomogeneous lithiation in V_2O_5 thin films with a non-integrated current collector.³³ The XPS mapping showed, at low current density, there was a uniform distribution of reduced vanadium from +5 state to +4 state over the distance measured from the current collector. At high current density, the vanadium near the current collector showed significantly higher reduced states than the rest of the film. When COMSOL Multiphysics was used to model this observation, the same XPS mapping of the vanadium states could not be fit using constant conductivity values reported for V_2O_5 . The distance over which

the reduction occurred indicated by the model was shorter than what was experimentally observed. Using dynamic conductivity, conductivity as a function of lithiation, the model was finally able to reproduce the experimental data. The reason was the increased conductivity of V_2O_5 during lithiation. The improved conductivity of V_2O_5 during lithiation led to a smaller drop in the overpotential throughout the electrode, leading to much better material usage further from the current collector. This explanation can also be adapted to describe the phenomenon that is observed with interconnections and the difference in the electrochemical properties of V_2O_5 .

The voltage profiles during the charge and discharge processes at 0.5C and 25C in both the one-Li ion and two-Li ion insertion regimes were analysed to further understand the mechanism for the different phenomenon observed between the electrodes with different numbers of interconnections. These can be seen in the supporting information (Figure S2 and S3). The profiles show the variances in electrochemical behavior between electrodes with zero and seven interconnecting layers. From the voltage profiles, the plateaus represent voltages where Li insertion and deinsertion and resulting phase transitions occur. To more clearly show these differences, first derivatives of the inverse of the voltage profiles were taken. The differential curve of the voltage profile is analogous to a cyclic voltammogram, and the peaks also correspond to the electrochemical reactions.⁴⁰ These can be seen in Figure 3b,c and Figure 4b,c for the one-Li and two-Li regimes respectively.

With 1 Li ion insertion, initially at low current densities, there is no significant influence of interconnecting layers on the capacity as the time scale is long enough for the electrodes to be lithiated uniformly, utilizing all the active material (Figure 3c). The peaks corresponding to each phase transition that occurs during lithiation and delithiation of V_2O_5 overlap for the electrodes with zero and seven interconnecting layers at 0.5C. However, as current density is increased, the electrodes are polarized due to relatively low electronic conductivity, leading to highly lithiated regions near the planar current collector. Within the 1 Li ion insertion regime, as stated before, the electronic conductivity increases with lithiation up to half Li then drops back to its initial conductivity when fully lithiated. At high current densities, however, as the electrodes are polarized, regions near the current collector are lithiated more than regions further away. With the interconnections, additional electronic pathways are introduced, which increases the overall distance electrons must travel. Due to the minimal conductivity change within the one-Li regime, and the longer electronic pathway from the interconnections, the electrode with seven interconnecting layers shows larger peak separation than the electrode with zero interconnecting layers at 25C in Figure 3C. Liu *et al.* also saw a similar effect with templated $LiFePO_4$ electrodes, where longer electron transport pathways resulted in higher overpotentials.³⁷ However, in our study the electrodes with seven interconnecting layers showed higher capacities than zero interconnecting layers within a one-Li insertion window. This observation could be explained by the full insertion and deinsertion peaks that are present in the differential plot of the electrode with seven interconnecting

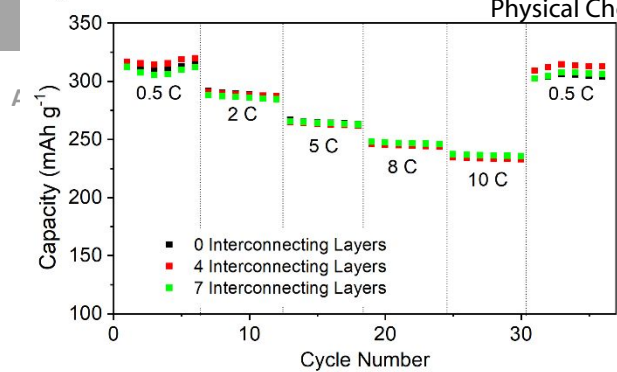


illustration of the difference in the degree of material utilization these interconnections may have. These images are not the result of calculations or simulations, rather they are presented to give a visual representation of what we propose is causing the changes in performance. Similar illustrations are provided later in this paper to help represent electrode changes under different conditions.

Another explanation for the electrode behavior differences could be that the Li ion diffusivity changes with degree of lithiation. As shown by McGraw et al., the diffusivity of Li ions in V_2O_5 indeed is also dynamic with lithiation.⁴¹ In order to experimentally resolve the impact of dynamic diffusivity and dynamic electronic conductivity, the structure of the current collector was varied from a planar Au current collector to an integrated Ru current collector. A thin layer of metallic Ru is deposited in the AAO templates via atomic layer deposition. The Ru coats the walls conformally as shown in a previous work.⁴² In the current study, a planar current collector was used meaning the electrons have to be transported along the material as far as $2.3 \mu\text{m}$ away from the current collector. However, with the integrated current collector, the electrons would travel through only the thickness of the active material, about 10 nm. If the dynamic electronic conductivity of the material plays a key role in the poor behavior of the electrode with the interconnections, with the integrated current collector there should be no difference in the capacities with varying numbers of interconnecting layers because electrons have a high conductivity pathway along the length of the electrode. Therefore, even if the conductivity of the V_2O_5 itself is poor, the integrated current collector will mitigate this negative effect. However, if it is the Li ion diffusivity that has a key role, integrated current collectors should have minimal impact on the electrochemistry and the difference in capacity retention should still be seen upon variation of the interconnecting layers. As shown in Figure 6, with an integrated current collector there is no difference between electrodes with zero and seven interconnecting layers. This result demonstrates that the differences in the capacities observed in Figure 4 are due to the negative synergistic behavior between the interconnecting layers and the dynamic conductivity of the active material. Figure 6b shows an illustration of proposed electrode structure with the intergraded current collector. This is purely an illustration to show the uniform lithiation that occurs due to the integrated current collector and not a mathematical simulation. These observations also suggest that in commercial electrodes with active materials that decrease in electronic conductivity upon lithiation such as LCO, the loss in capacity could be due to the loss in the electronic conductance.

The impact of interconnecting layers on the degradation of the electrode was also explored. With a planar current collector, there is a difference in the degradation rate between zero interconnecting layers and seven interconnecting layers. To better represent the degradation of the electrodes, the capacities were normalized to the first cycle. While this data shows that with more interconnecting layers the capacity degrades at a faster rate, the mechanism for the degradation is unclear. There are two possibilities for the degradation in this

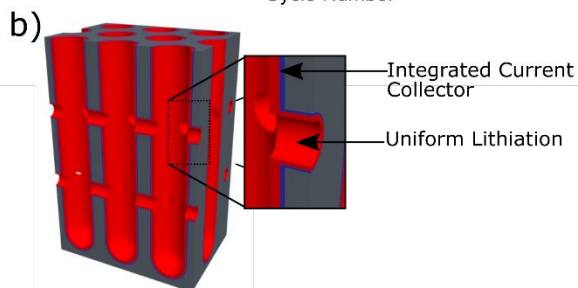


Fig. 6 (a) Capacity of V_2O_5 of electrodes with various interconnecting layer, cycled between 2 V and 4V vs Li with integrated Ru current collector (b) Proposed uniform lithiation with integrated current collector

layers, which still shows a high degree of material utilization. There is more material closer to the planar current collector with more interconnections, which leads to the higher capacity at 25C. This result demonstrates a positive synergistic behavior between the interconnecting layers and the electronic conductivity of the active material with lithiation, leading to better capacities at higher current densities.

A similar explanation can be used for the negative synergistic behavior between the interconnecting layers and the decrease in the electronic conductivity of the active material, which is the case for the two-Li insertion regime. At lower current densities, there is minimal polarization of the electrode, thus enabling V_2O_5 to be fully lithiated, leading to similar specific capacities with varying numbers of interconnecting layers. The differential plot for the 2 Li ion insertion region plotted in Figure 4b illustrates the three distinct phase transition peaks for a total of 2 Li ion insertions into V_2O_5 at 0.5C. There is no clear difference between the electrodes with zero and seven interconnecting layers, again supporting this explanation. When the current density is increased, similar to the one-Li case, the electrode becomes more polarized. However, instead of having similar electronic conductivity during lithiation of the V_2O_5 , it significantly decreases with lithiation, leading to even higher degree of electrode polarization. As can be seen in Figure 4c, there is a significant amount of peak separation at 25C for both electrodes. For the one with zero interconnecting layers, the five phase transition peaks can still be seen even though large electrochemical irreversibility is seen. For the electrode with seven interconnecting layers, not only there is the additional electronic pathways the electrons need to travel but these pathways become further electronically insulating with further lithiation of the V_2O_5 , reducing the amount of active material that can be utilized in the electrode further away from the current collector. In Figure 4c, the electrode with seven interconnecting layers shows only partial phase transitions due the severe peak separations, thus upon reaching the upper and lower voltage limits peaks are cut off. Figure S4 shows an

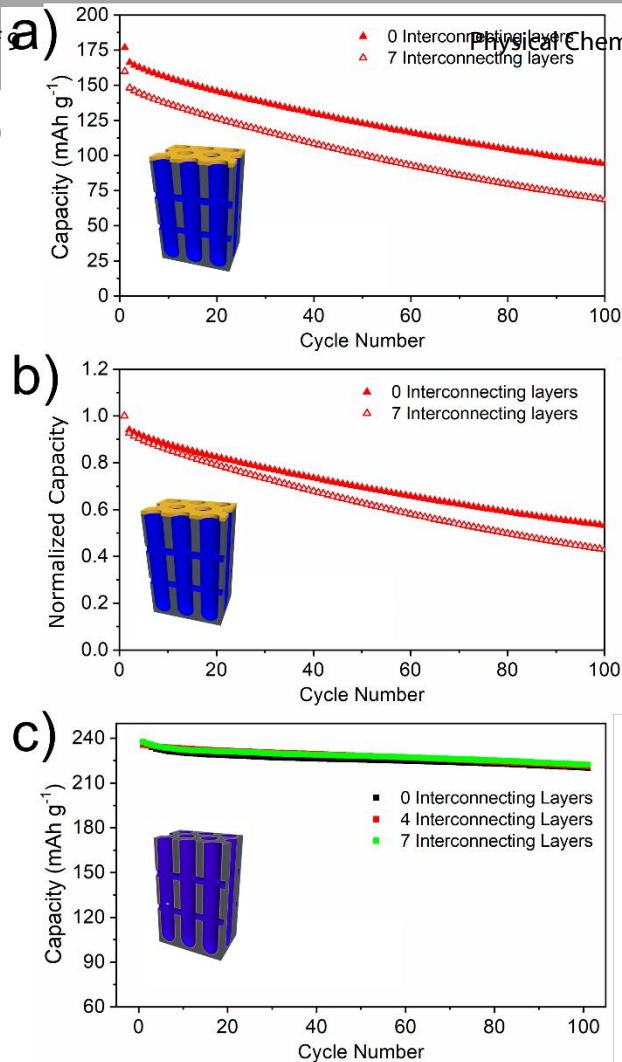


Fig. 7 Gravimetric cycling at 10C (a) with planar current collector and (c) with integrated current collector with different numbers of interconnecting layers (b) shows normalized capacity of (a) respective to the first cycle.

system. The first possibility is the structural irregularities due to the interconnections, which may result in sharp edges and corners where electrochemical hotspots could form, leading to irreversible reactions (for V_2O_5 , the 3rd Li insertion is). To understand the irreversible reactions, it is important to understand the various phase changes of V_2O_5 upon lithiation. Pristine V_2O_5 is in the α phase. From zero Li ion to one Li ion insertion, V_2O_5 goes through reversible phase transitions from α to ϵ , then ϵ to δ phase. From one to two Li ions, the δ phase transforms into γ due to the breaking of some V-O bonds to accommodate the second Li ion. While this phase transition is irreversible, all Li ions can still be reversibly removed and re-intercalated into the γ phase. When more than two Li ions are inserted, another phase transition occurs into the ω phase to accommodate additional Li ions. This change to a rock-salt structure is irreversible not only with regard to the crystalline phase transition, but also the large amount of Li ions that cannot be removed after insertion, thus lowering the energy density after three Li ions are inserted.^{29, 43, 44} The other is due to the electrode polarization where to maintain the required current densities, high overpotentials are applied to the active material closer to the current collector, again resulting in irreversible reactions. The use of the two different current collector structures allows the separation of these two mechanisms. The electrochemical hotspots are the result of sharp edges where the electric field is the highest. By providing

an integrated current collector, the electric field at these sharp edges should be enhanced, thus lead to further irreversible reactions. However, it can be seen in Fig 7 that with the integrated current collector no difference in the degradation can be seen. This outcome suggests that the degradation mechanism, despite the structure irregularities of the interconnecting layers, are likely due to the polarization of the electrode.

Conclusion

In this study, well controlled nanostructured electrodes were fabricated to understand the complex interactions between structure and its impact on the ion and electron pathways which determine the electrochemical behavior of the electrode. Differing behaviors were observed between electrodes with and without interconnecting layers in one and two Li insertion regimes. In the one-Li insertion regime, electrodes with seven interconnecting layers showed about 5% higher capacity than electrodes with zero interconnections at 25C, whereas in the two-Li insertion regime, electrodes with seven interconnecting layers showed about 20% less capacity than those with zero interconnections at 25C. To understand the impact of the interconnections within the different Li insertion regimes on the electrode capacity, the pore diameters of the electrodes were first changed. While larger pore diameter showed higher capacities overall, it still showed that in the two-Li insertion regime, fewer interconnections led to higher capacities. To understand whether the capacities were limited by the dynamic electronic conductivity or dynamic Li diffusivity, an integrated current collector was used. With the integrated current collector, no difference in capacity was seen among samples with varying numbers of interconnections, showing that the difference between the electrodes with interconnecting layers in the two different regimes were from the positive and negative synergistic behavior of the electronic conductivity and interconnections. The impact of the structural irregularities from the interconnections on the degradation rate was also investigated. From constant GV cycling at 25C, the electrodes with seven interconnecting layers lost 10% more capacity than the electrodes without any interconnections. Further, this was supported by experiments with integrated current collectors where these samples demonstrated the same capacities with increased current densities independent of how many interconnections were present, thus that the polarization of the electrode was the source of the increased degradation.

This study demonstrates that material properties must be carefully chosen due to the observation that within the same electrode architecture, dynamic materials' properties can either help or harm the electrochemical characteristics of the electrode depending on how the properties change during ion insertion. It was also shown that the irregularities caused by the interconnections did not have a significant impact on the degradation mechanism, whereas the polarization of the electrode was found to be the major contributor to the electrode degradation. This well controlled 3D porous electrode structure can be further used as test bed platform to examine

the impact of additional ionic and electronic path ways in different battery material with varying battery chemistries.

Conflicts of interest

There are no conflicts to declare.

Acknowledgements

The acknowledgements come at the end of an article after the conclusions and before the notes and references. We acknowledge the support of the Maryland Nanocenter, its Fablab, and its AIMLab. This work was supported as part of the Nanostructures for Electrical Energy Storage (NEES), an Energy Frontier Research Center (EFRC) funded by the U.S. Department of Energy, Office of Science, Office of Basic Energy Sciences under Award Number DESC0001160

References

1. Y. Zhang, H. Feng, X. B. Wu, L. Z. Wang, A. Q. Zhang, T. C. Xia, H. C. Dong, X. F. Li and L. S. Zhang, *Int. J. Hydrogen Energy*, 2009, **34**, 4889-4899.
2. P. Simon and Y. Gogotsi, *Nat. Mater.*, 2008, **7**, 845-854.
3. C. Liu, F. Li, L. P. Ma and H. M. Cheng, *Adv. Mater.*, 2010, **22**, E28-E62.
4. E. Detsi, X. Petrissans, Y. Yan, J. B. Cook, Z. Deng, Y.-L. Liang, B. Dunn and S. H. Tolbert, *Phys. Rev. Mater.*, 2018, **2**, 055404.
5. C. S. Choi, J. Lau, J. Hur, L. Smith, C. Wang and B. Dunn, *Adv. Mater.*, 2017, **30**, 1703772.
6. L. Jin, B. Liu, Y. Wu, S. Thanneeru and J. He, *ACS Appl. Mater. Interfaces*, 2017, **9**, 36837-36848.
7. J. R. Swierk, N. S. McCool, C. T. Nemes, T. E. Mallouk and C. A. Schmuttenmaer, *J. Phys. Chem. C*, 2016, **120**, 5940-5948.
8. V. Muenzel, A. F. Hollenkamp, A. I. Bhatt, J. de Hoog, M. Brazil, D. A. Thomas and I. Mareels, *J. Electrochem. Soc.*, 2015, **162**, A1592-A1600.
9. T. Hayashi, J. Okada, E. Toda, R. Kuzuo, N. Oshimura, N. Kuwata and J. Kawamura, *J. Electrochem. Soc.*, 2014, **161**, A1007-A1011.
10. J. H. Park, S. W. Kang, T. S. Kwon and H. S. Park, *Ceram. Int.*, 2018, **44**, 2683-2690.
11. S. Ozkan, G. Cha, A. Mazare and P. Schmuki, *Nanotechnology*, 2018, **29**, 195402.
12. A. H. Wiedemann, G. M. Goldin, S. A. Barnett, H. Y. Zhu and R. J. Kee, *Electrochim. Acta*, 2013, **88**, 580-588.
13. D. W. Chung, P. R. Shearing, N. P. Brandon, S. J. Harris and R. E. Garcia, *J. Electrochem. Soc.*, 2014, **161**, A422-A430.
14. J. R. Wilson, J. S. Cronin, S. A. Barnett and S. J. Harris, *J. Power Sources*, 2011, **196**, 3443-3447.
15. S. J. Cooper, D. S. Eastwood, J. Gelb, G. Damblanc, D. J. L. Brett, R. S. Bradley, P. J. Withers, P. D. Lee, A. J. Marquis, N. P. Brandon and P. R. Shearing, *J. Power Sources*, 2014, **247**, 1033-1039.
16. M. Shibuya, T. Nishina, T. Matsue and I. Uchida, *J. Electrochem. Soc.*, 1996, **143**, 3157-3160.
17. M. Le, Y. Liu, H. Wang, R. K. Dutta, W. B. Yan, J. C. Hemminger, R. Q. Q. Wu and R. M. Penner, *Chem. Mater.*, 2015, **27**, 3494-3504.
18. T. Hutzenlaub, S. Thiele, N. Paust, R. Spotnitz, R. Zengerle and C. Wachsofer, *Electrochim. Acta*, 2014, **115**, 131-139.
19. W. Lee and S. J. Park, *Chem. Rev.*, 2014, **114**, 7487-7556.
20. J. Oh and C. V. Thompson, *Adv. Mater.*, 2008, **20**, 1368-1372.
21. L. Y. Wen, R. Xu, Y. Mi and Y. Lei, *Nat. Nanotechnol.*, 2017, **12**, 244-252.
22. J. Martín, M. Martín-González, J. Francisco Fernández and O. Caballero-Calero, *Nat. Commun.*, 2014, **5**, 5130-5138.
23. E. Gillette, S. Wittenberg, L. Graham, K. Lee, G. Rubloff, P. Banerjee and S. B. Lee, *Phys. Chem. Chem. Phys.*, 2015, **17**, 3873-3879.
24. P. M. Resende, R. Sanz, A. Ruiz-de Clavijo, O. Caballero-Calero and M. Martín-González, *Coatings*, 2016, **6**, 59.
25. E. I. Gillette, N. Kim, G. W. Rubloff and S. B. Lee, *Phys. Chem. Chem. Phys.*, 2016, **18**, 30605-30611.
26. S. J. Harris and P. Lu, *J. Phys. Chem. C*, 2013, **117**, 6481-6492.
27. Z. Li, J. Huang, B. Y. Liaw, V. Metzler and J. B. Zhang, *J. Power Sources*, 2014, **254**, 168-182.
28. L. Enze, *J. Phys. D: Appl. Phys.*, 1986, **19**, 1-6.
29. J. H. Yao, Y. W. Li, R. C. Masse, E. Uchaker and G. Z. Cao, *Energy Storage Mater.*, 2018, **11**, 205-259.
30. C. F. Armer, M. Lubke, M. V. Reddy, J. A. Darr, X. Li and A. Lowe, *J. Power Sources*, 2017, **353**, 40-50.
31. R. Baddour-Hadjean, V. Golabkan, J. P. Pereira-Ramos, A. Mantoux and D. Lincot, *J. Raman Spectrosc.*, 2002, **33**, 631-638.
32. C. K. Chan, H. L. Peng, R. D. Twisten, K. Jarausch, X. F. Zhang and Y. Cui, *Nano Lett.*, 2007, **7**, 490-495.
33. A. J. Pearse, E. Gillette, S. B. Lee and G. W. Rubloff, *Phys. Chem. Chem. Phys.*, 2016, **18**, 19093-19102.
34. S. Dierks, Vanadium Oxide V₂O₅ Material Safety Data Sheet, <http://www.espietals.com/index.php/msds/303-vanadium-oxide-v2o5>, (accessed 10/08, 2018).
35. K. Kitada, H. Murayama, K. Fukuda, H. Arai, Y. Uchimoto, Z. Ogumi and E. Matsubara, *J. Power Sources*, 2016, **301**, 11-17.
36. N. Ogihara, Y. Itou, T. Sasaki and Y. Takeuchi, *J. Phys. Chem. C*, 2015, **119**, 4612-4619.
37. Z. Liu, T. W. Verhallen, D. P. Singh, H. Q. Wang, M. Wagemaker and S. Barnett, *J. Power Sources*, 2016, **324**, 358-367.
38. M. Shibuya, S. Yamamura, T. Matsue and I. Uchida, *Chem. Lett.*, 1995, 749-750.
39. C. Julien, *New Trends in Intercalation Compounds for Energy Storage*, 2016.
40. E. Talaie, P. Bonnicks, X. Q. Sun, Q. Pang, X. Liang and L. F. Nazar, *Chem. Mater.*, 2017, **29**, 90-105.
41. J. M. McGraw, C. S. Bahn, P. A. Parilla, J. D. Perkins, D. W. Readey and D. S. Ginley, *Electrochim. Acta*, 1999, **45**, 187-196.
42. C. Y. Liu, E. I. Gillette, X. Y. Chen, A. J. Pearse, A. C. Kozen, M. A. Schroeder, K. E. Gregorczyk, S. B. Lee and G. W. Rubloff, *Nat. Nanotechnol.*, 2014, **9**, 1031-1039.
43. R. Baddour-Hadjean and J. P. Pereira-Ramos, *Chem. Rev.*, 2010, **110**, 1278-1319.

Journal Name

ARTICLE

44. K. Kalaga, F. N. Sayed, M. T. F. Rodrigues and P. M. Ajayan, *Jom*, 2017, **69**, 1509-1512.